



Identifying critically stressed faults without triggering slip : A discussion

David Eaton, Mason Mackay, Anton Biryukov, Murad S. Abuaisha

► To cite this version:

David Eaton, Mason Mackay, Anton Biryukov, Murad S. Abuaisha. Identifying critically stressed faults without triggering slip : A discussion. Microseismic Industry Consortium: Annual Research Report, Volume 6, 2016. hal-02461099

HAL Id: hal-02461099

<https://minesparis-psl.hal.science/hal-02461099>

Submitted on 30 Jan 2020

HAL is a multi-disciplinary open access archive for the deposit and dissemination of scientific research documents, whether they are published or not. The documents may come from teaching and research institutions in France or abroad, or from public or private research centers.

L'archive ouverte pluridisciplinaire **HAL**, est destinée au dépôt et à la diffusion de documents scientifiques de niveau recherche, publiés ou non, émanant des établissements d'enseignement et de recherche français ou étrangers, des laboratoires publics ou privés.

Chapter 35

Identifying critically stressed faults without triggering slip: A discussion

David W. Eaton^a, Mason MacKay^a, Anton Biryukov^a and Murad AbuAisha^a

^a *Department of Geoscience, University of Calgary, Calgary, AB, T2N 1N4, Canada.
E: eatond@ucalgary.ca*

Summary

Identifying and mapping critically stressed faults is a key first step for assessing hazards from induced seismicity. The classical paradigm of mapping faults with seismic or well log data may not be universally successful, however, as faults are sometimes cryptic and not easily identified. This is especially true for near-vertical strike-slip faults, for which vertical reflection offsets and/or diffractions may not be conspicuous, or in the case of low-angle thrust faults such as an intracutaneous wedge within a thick shale sequence. We propose alternative approaches for identifying critically stressed faults that involve: 1) modeling and mapping of stress perturbations caused by the presence of a critically stressed fault system, 2) mapping localized zones of anomalous pore pressure in a target shale formation, and 3) dynamic triggering of microseismicity due to high-amplitude surface waves resulting from large teleseismic earthquakes. The goal of this work is to promote further discussion.

35.1 Introduction

The identification and mapping of potential seismogenic faults without activating them is an important element for risk assessment for injection-induced seismicity (Walters et al., 2015). Traditionally, the identification of faults is carried out using well logs (Rafiq et al., 2016) or by mapping reflection offsets in seismic profiles (Figure 1). However, this approach is not always viable, especially in the case of near-vertical strike-slip faults or sub-horizontal faults. Strike-slip faults commonly have a near-vertical fault orientation and may not result in any obvious vertical offset across the fault. Moreover, thrust-fault systems commonly contain low-angle (flat) segments. If such segments occur within a thick shale sequence they may be difficult to identify.

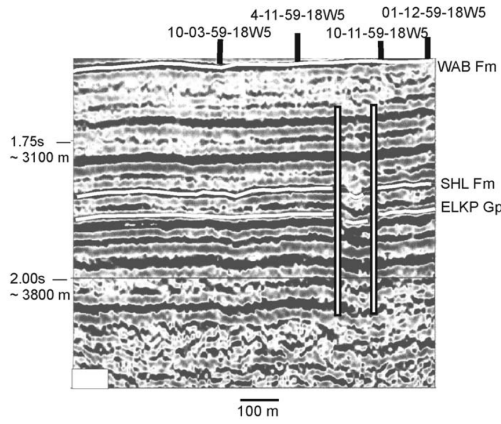


Figure 1: Seismic line in the Fox Creek region showing interpreted faulting. From Green and Mountjoy, 2005.

In this paper, we propose alternative approaches to identification of critically stressed faults. These alternative approaches consist of:

1. Mapping perturbations in stress conditions near a fault, including changes in stress magnitude and direction (Figure 2). Such variations in stress could be identified using DFIT, wellbore breakouts (Bell et al., 1992) and cross-dipole sonic logs. Under favourable conditions it may be possible to map stress variations in detail using seismic data that is calibrated using these independent sources.
2. Mapping pore pressure compartments within a reservoir. We propose that faults may act as barriers to stress equalization within a reservoir.
3. Identifying critically stressed faults by mapping microearthquakes that are dynamically triggered by the passage of large-amplitude surface waves from distant earthquakes. Implementation of this approach would require deployment of a seismograph array in advance of hydraulic fracturing.

These three proposed methods are examined in the following sections.

35.2 Stress Modeling

In order to calculate how the stress field around a fault is perturbed both in magnitude and direction, the finite-difference code FLAC3D was used (Itasca, 2012). The finite-difference approach allows for materials to be represented as cubic polyhedral elements that are free to deform following Hooke's elastic constitutive law (Itasca, 2012),

$$\Delta\sigma_{ij} = 2G\Delta\epsilon_{ij} + \left(K - \frac{2}{3}G\right) \Delta\epsilon_{kk}\delta_{ij}, \quad (35.1)$$

where Einstein notation is used implying the change in stress is a function of the Kronecker delta δ_{ij} , bulk modulus, K , and shear modulus G . An elastic material formulation without a failure criterion was used in order to represent the complete mechanics of stress distribution around a fault without the complexity of failure mechanisms that one would expect to be associated with dynamic processes.

The model approximates a stress condition that is characterized by both strike slip and thrust fault regimes based on the critically stressed crust theorem, wherein the ratio of maximum and minimum principal stresses, σ_1 to σ_3 is dependent on a coefficient of friction, μ , of 0.6 (Zoback 2010):

$$\frac{\sigma_1}{\sigma_3} = \left(\sqrt{\mu^2 + 1} + \mu^2\right)^2. \quad (35.2)$$

The convention used by the numerical code is that negative stresses are compressive. The stress state is at a modelled depth of 3 km assuming an average crustal density of 2700 kg/m³ and a hydrostatic pore pressure gradient. The fault is approximated as a circle with a diameter of 3 km and the model size is 12 × 12 × 12 km. The 25 m computational grid is gradationally meshed in order to balance computation time and numerical accuracy with mesh elements at the fault face. The material properties and model parameters are summarized in Table 1.

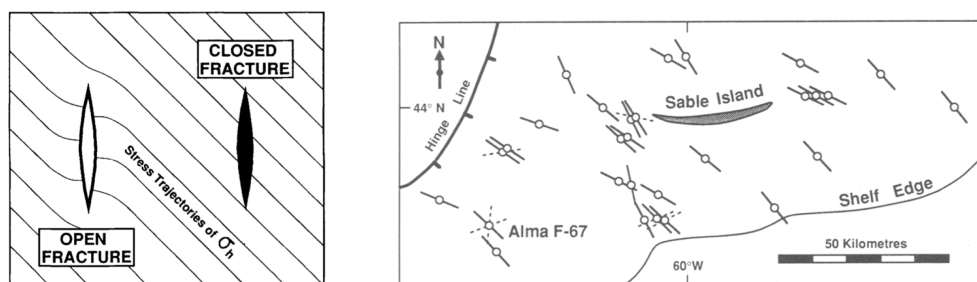


Figure 2: Left panel: deflection of maximum horizontal stress orientation in the neighbourhood of vertical open fractures that are not oriented perpendicular to the smallest principal stress. Right panel: deflection of mean borehole breakout azimuths from 29 wells in the Scotian Shelf, offshore eastern Canada. From Bell et al., 1992.

The effects of gravity were neglected and the model was initialized with an in situ stress state. Boundary conditions were applied with fixed corners and constrained to only allow for shear displacement at the model boundary. The model was then stepped to equilibrium and the fault region material was changed to a weaker material by assigning a fault material with half the bulk and shear modulus of the surrounding rockmass. The model was then stepped to a new equilibrium and analysis of the stress perturbation was made. The results of stress modelling are summarized in Figures 3-5.

35.3 Pore pressure compartments

In sedimentary basins, regions of pore overpressure can be compartmentalized by permeability barriers (Hunt, 1990). Breaches in integrity of seals can occur due to fracturing, induced by generation of hydrocarbons within the compartments and/or the thermal expansion of pore fluids. An episodic process of resealing and breakout cycles in intervals of thousands of years has been proposed by Hunt (1990). Figure 6 shows an example of compartmentalized pore overpressure within the Montney region of Alberta and British Columbia and its possible relationship to anomalous induced seismicity (Eaton et al., this volume).

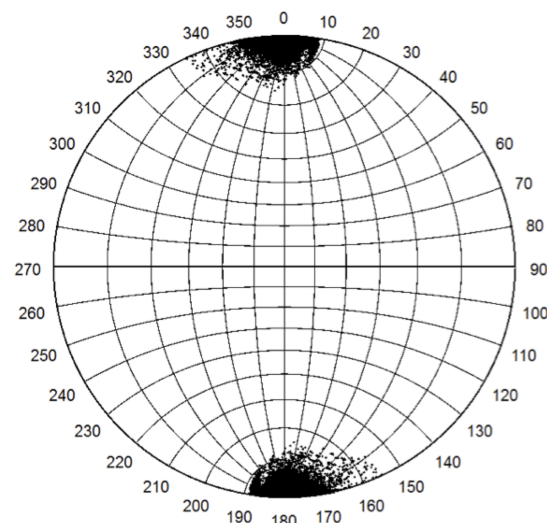


Figure 5: Maximum principal stress rotation. Points represent trends and plunge of the primary principal stress orientation. Deviation from a perfect North to south alignment indicates a rotation of the stress field by up to 25 degrees.

Table 1: FLAC3D fault zone modelling parameters. The following parameters are chosen to represent the rockmass and fault properties of an assumed fault zone that may be a candidate for induced seismicity.

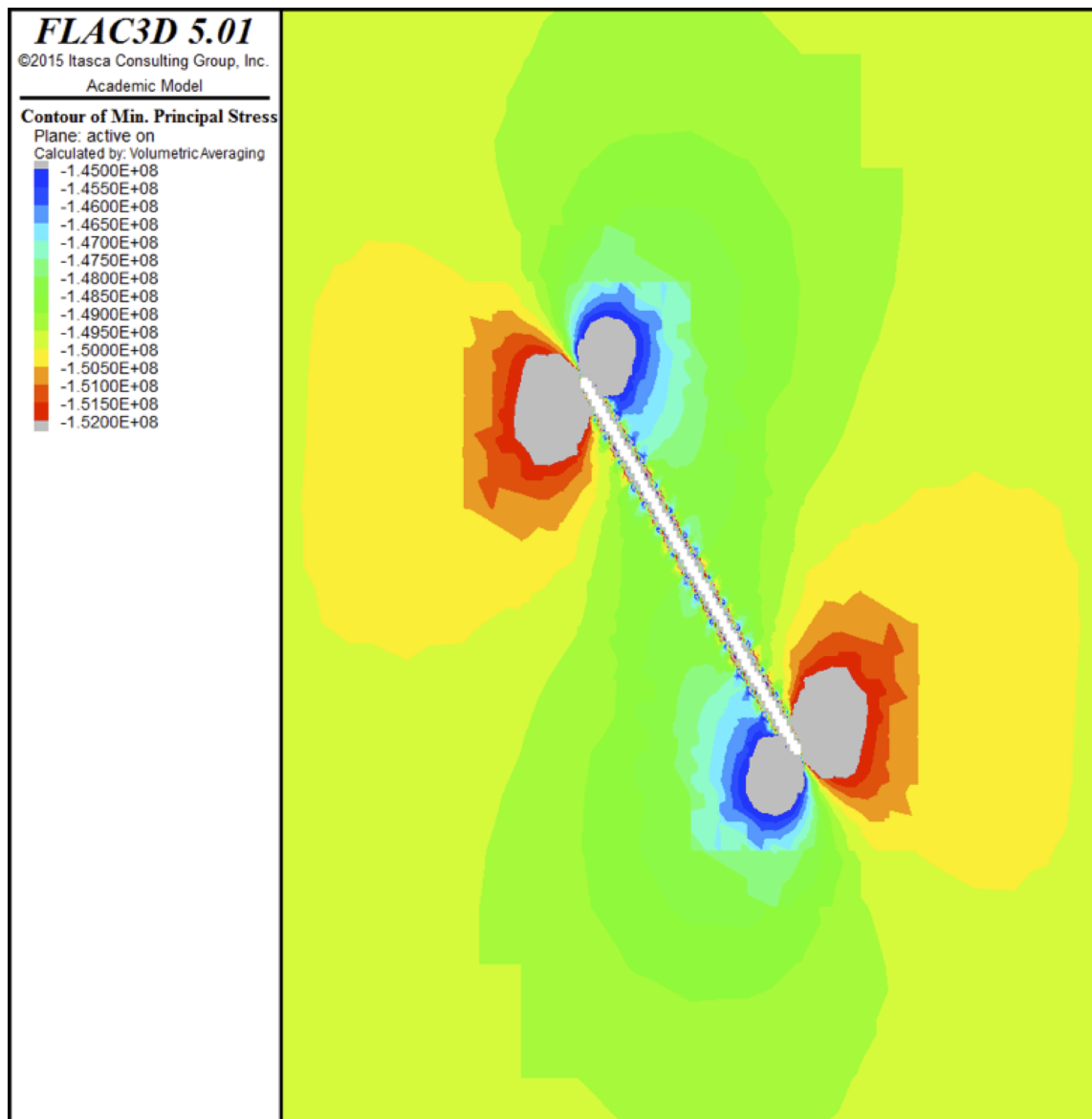


Figure 3: Maximum principal stress magnitudes contours around a 3 km fault. Stress perturbations indicate a lowering of stress magnitudes in the core of the fault with increase stress magnitude lobes distally from the fault edges.

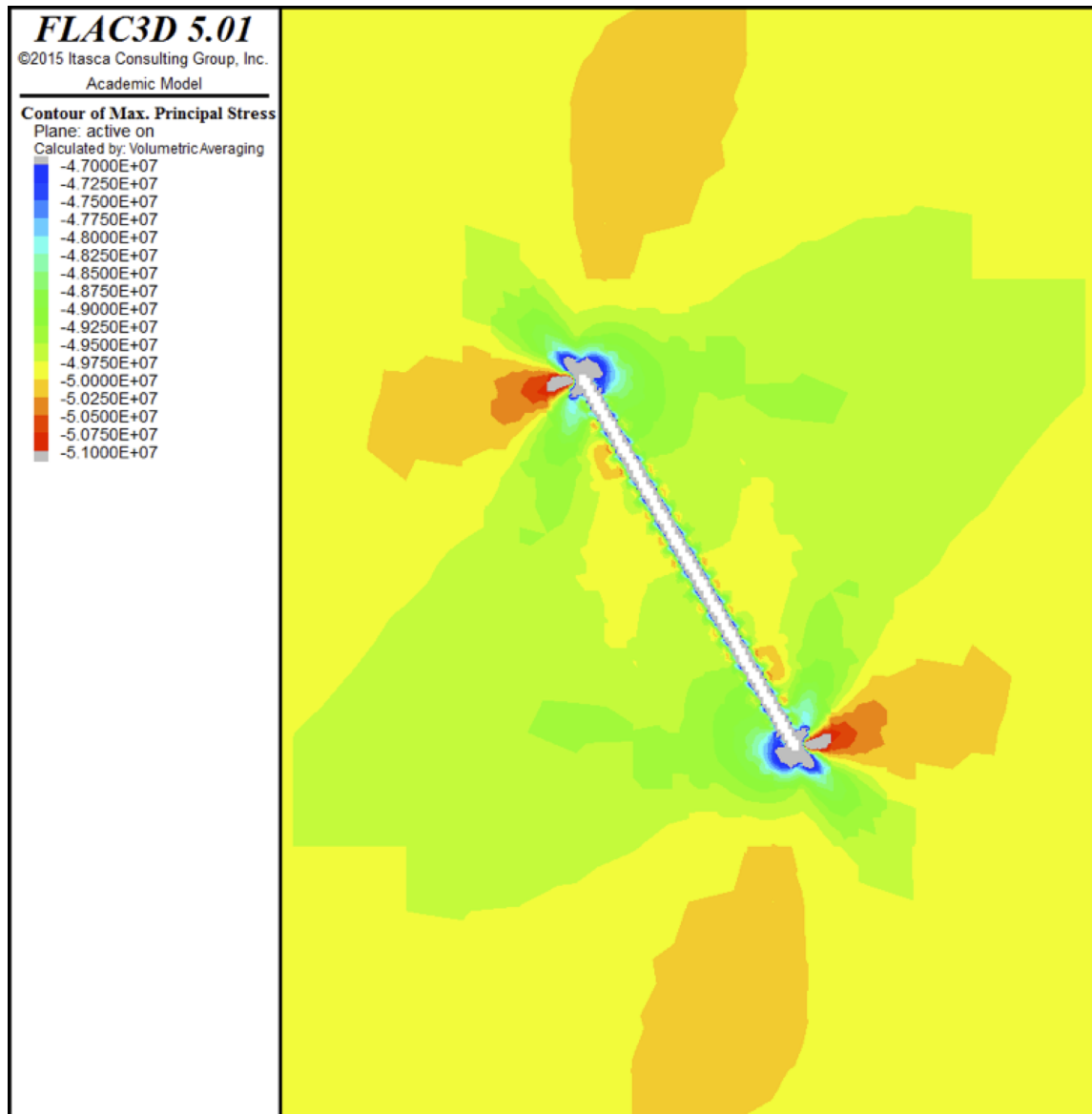


Figure 4: Minimum principal stress magnitude contours. Increased compressive stresses (orange) are observed distally to the fault, while zones of relaxation (green) occur in other regions.

Model Parameters	Value	Units
Density	2700	kg/m ³
Principal stress magnitudes	-150, -50, -50	MPa
Shmax (trend/plunge)	180/0	degrees
Shmin (trend/plunge)	90/0	degrees
Bulk modulus K	20	GPa
Shear modulus G	12	GPa
Fault diameter	3	km
Fault zone width	60	m

In other cases, earthquakes occurring weeks to months after the initial earthquake have been interpreted as a delayed response to dynamic triggering.

Recently, van der Elst et al. (2013) and Wang et al. (2015) noticed that seismic activity on a fault in the areas of wastewater injection may be related to the stress perturbations caused by strong distant earthquakes. By using the novel match-filtering approach, they have managed to extract low-magnitude events from the continuous waveform data and establish the statistical causality between the major distant earthquakes and local increase in the seismic activity in the hydraulically stimulated areas.

35.4 Dynamic Triggering

Dynamic triggering happens as surface seismic waves from an initial earthquake propagate through the Earth's crust and perturb the stresses at local critically stressed faults, triggering secondary earthquakes. Once the seismic wave train has passed and ground shaking ends, the crust in the local area returns to its previous stress state modified according to the cumulative stress drops associated with locally triggered earthquakes.

Dynamic triggering of secondary earthquakes was widely accepted in the scientific community following the 1992 M7.3 Landers earthquake in southern California. Earthquake rates increased dramatically across the western United States at distances well beyond the after-shock zone in a few days after the earthquake (Hill et al., 1993). Furthermore, dynamic triggering has been observed across the globe in various geologic and tectonic environments. It has been shown to take place at distances from the initial rupture varying from meters (Kilb et al., 2000) to over thousands of kilometers (West et al., 2005). The main ruptures have been noticed to trigger other earthquakes at different time scales. In many cases secondary earthquakes occurred within minutes to hours following the primary seismic surface wave arrival (West et al., 2005; Gomberg et al., 2004).

Having been located and shown on the map, the series of triggered event locations may be spatially clustered, thus providing an estimate of the dimensions of the fault that has undergone dynamic triggering. This suggests that such remote triggering could potentially serve as a probe for outlining the areas where critically stressed faults are present, prior to any hydrocarbon field development. This procedure could serve as a preventive manner of accidental fault activation, causing unnecessary slip, and thus reduce the risk of a production disruption.

35.5 Conclusions and Outlook

Recognition and mapping of critically stressed faults is a key component of hazard assessment for anomalous induced seismicity. Under various common circumstances, fault imaging and mapping may be problematic using traditional methods, including 3-D seismic imaging or mapping with densely spaced well log data. We propose three novel methods for indirectly inference of the existence and location of critically stressed faults: mapping perturbations to regional stress, mapping compartments in pore pressure, and clustering of naturally occurring microearthquakes that are dynamically triggered by teleseismic surface waves. Ongoing research is focused on evaluation of the potential utility

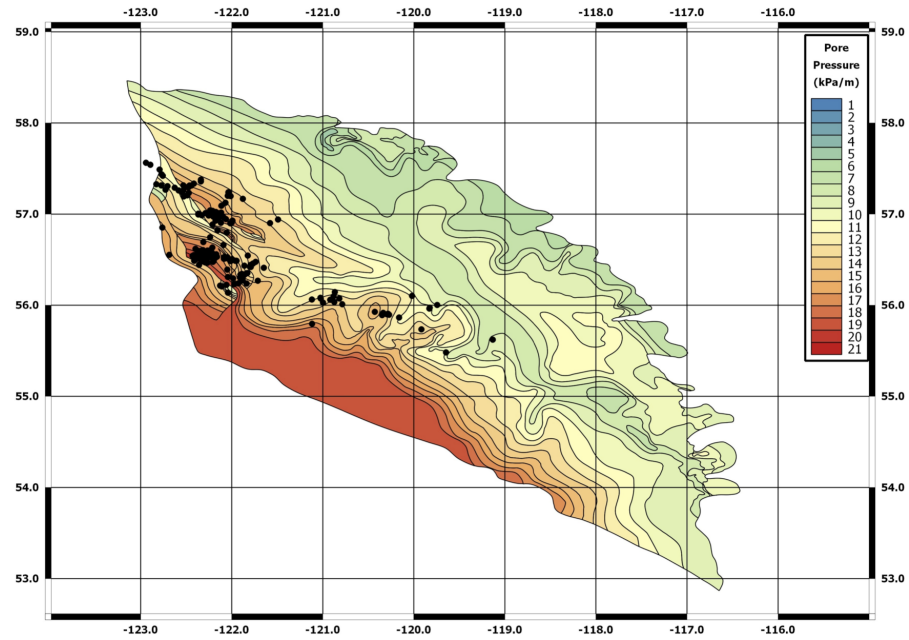


Figure 6: Heterogeneous (compartmentalized) pore-pressure gradient in the Montney trend, courtesy Canadian Discovery, Ltd. Black dots show $M \geq 2.5$ earthquakes since 2008, suggesting that pore-pressure compartments may be linked to faults.

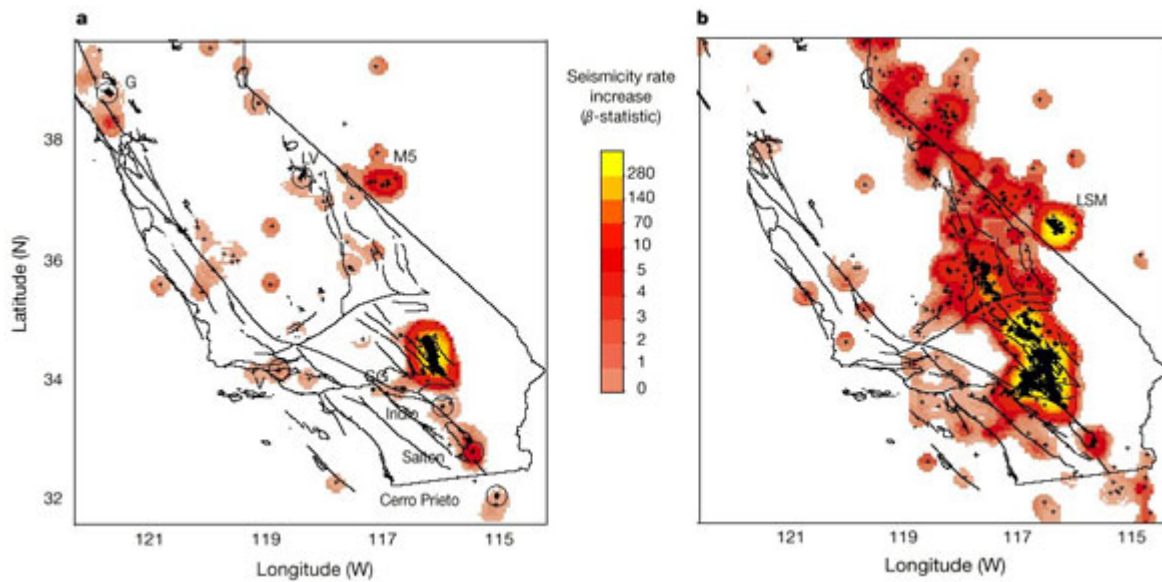


Figure 7: Seismicity rate increases associated with Hector Mine and Landers mainshocks, showing that dynamically triggered events tend to align along faults. From Gomberg et al. (2001).

of these proposed methods.

35.6 Acknowledgments

Sponsors of the Microseismic Industry Consortium are thanked for their long-standing support of this research topic. We are particularly grateful to Canadian Discovery Ltd. for permission to show the pore-pressure data, as well as the Natural Sciences and Engineering Research Council of Canada (NSERC) and Chevron Canada for their support of an Industrial Research Chair in Microseismic System Dynamics at the University of Calgary. In addition, Aquaterra Water Management, ConocoPhillips Canada, Microseismic Canada and Nanometrics are thanked for sponsorship of a collaborative research program on multi-scale monitoring of hydraulic fracturing and wastewater injection, Duvernay region.

35.7 References

- Bell, J.S., G. Caillet and J. Adams, 1992. Attempts to detect open fractures and non-sealing faults with dipmeter logs. Geological Society Special Publication, **65**, 211-220.
- Eaton, D., B. Cheadle and A. Fox, 2016. A causal link between overpressured hydrocarbon source rocks and seismicity induced by hydraulic fracturing. This volume.
- Green, D.G. and E.W. Mountjoy, 2005. Fault and conduit controlled burial dolomitization of the Devonian west-central Alberta Deep Basin. Bulletin of Canadian Petroleum Geology, **53**, 101-129.
- Gomberg, J., P. A. Reasenber, P. Bodin and R. A. Harris, 2001. Earthquake triggering by seismic waves following the Landers and Hector Mine earthquakes Nature, **411**, 462-466.
- Gomberg, J., Bodin, P., Larson, K., and Dragert, H., 2004. Earthquake nucleation by transient deformations caused by the M = 7.9 Denali, Alaska, earthquake. Nature, **427**, 621-624.
- Hill, D. P., Reasenber, P. A., Michael, A., Arabaz, W. J., Beroza, G., Brumbaugh, D., Brune, J. N., Castro, R., Davis, S., and Depolo, D., 1993. Seismicity remotely triggered by the magnitude 7.3 Landers, California, earthquake. Science, **260**, 1617-1623.
- Hunt, J.M., 1990. Generation and Migration of Petroleum from Abnormally Pressured Fluid Compartments. AAPG Bulletin, **74**, 1-12.
- Itasca Consulting Group, Inc., 2012. FLAC3D - Fast Lagrangian Analysis of Continua in Three-Dimensions. Ver. 5.0. Minneapolis: Itasca.
- Kilb, D., Gomberg, J., and Bodin, P., 2000. Triggering of earthquake aftershocks by dynamic stresses. Nature, **408**, 570-574.
- Rafiq, A., D.W. Eaton, A. McDougall and P.K. Pederson, 2016. Reservoir Characterization using Microseismic Facies Analysis Integrated with Surface Seismic Attributes, Interpretation, in press.
- van der Elst, N. J., Savage, H. M., Keranen, K. M., and Abers, G. A., 2013. Enhanced Remote Earthquake Triggering at Fluid-Injection Sites in the Midwestern United States. Science, **341**, 164-167.
- Wang, B., Harrington, R. M., Liu, Y., Yu, H., Carey, A., and van der Elst, N. J., 2015. Isolated cases of remote dynamic triggering in Canada detected using cataloged earthquakes combined with a matched-filter approach. Geophysical Research Letters, **42**, 2015GL064377.
- Walters, R.J., Zoback, M.D., Baker, J.W. and Beroza, G.C., 2015. Characterizing and Responding to Seismic Risk Associated with Earthquakes Potentially Triggered by Fluid Disposal and Hydraulic Fracturing. Seismological Research Letters, **86**, 1110-1118.
- West, M., Sanchez, J. J., and McNutt, S. R., 2005. Periodically Triggered Seismicity at Mount Wrangell, Alaska, after the Sumatra Earthquake. Science, **308**, 1144-1146.
- Zoback, M. D., 2010. Reservoir geomechanics. Cambridge University Press.